

Quantum spin nematic phase in a square-lattice iridate

Hoon Kim,^{1,2,*} Jin-Kwang Kim,^{1,2,*} Jimin Kim,^{1,2} Hyun-Woo J. Kim,^{1,2} Seunghyeok Ha,^{1,2}
Kwangrae Kim,^{1,2} Wonjun Lee,^{1,2} Jonghwan Kim,^{3,4} Gil Young Cho,^{1,2} Hyeokjun Heo,⁵ Joonho Jang,⁵
J. Strempler,⁶ G. Fabbri,⁶ Y. Choi,⁶ D. Haskel,⁶ Junggho Kim,⁶ J. W. Kim,⁶ and B. J. Kim^{1,2,†}

¹Center for Artificial Low Dimensional Electronic Systems,
Institute for Basic Science (IBS), 77 Cheongam-Ro, Pohang 37673, South Korea

²Department of Physics, Pohang University of Science and Technology, Pohang 37673, South Korea

³Center for Van der Waals Quantum Solids, Institute for Basic Science (IBS), Pohang, 37673, Korea

⁴Department of Materials Science and Engineering,
Pohang University of Science and Technology, Pohang 37673, Korea

⁵Department of Physics and Astronomy, Seoul National University, Seoul 08826, South Korea

⁶Advanced Photon Source, Argonne National Laboratory, Argonne, Illinois 60439, USA

(Dated: December 15, 2023)

Spin nematic (SN) is a magnetic analog of classical liquid crystals, a fourth state of matter exhibiting characteristics of both liquid and solid^{1,2}. Particularly intriguing is a valence-bond SN³⁻⁶, in which spins are quantum entangled to form a multi-polar order without breaking time-reversal symmetry, but its unambiguous experimental realization remains elusive. Here, we establish a SN phase in the square-lattice iridate Sr₂IrO₄, which approximately realizes a pseudospin one-half Heisenberg antiferromagnet (AF) in the strong spin-orbit coupling limit⁷⁻¹⁰. Upon cooling, the transition into the SN phase at $T_C \approx 263$ K is marked by a divergence in the static spin quadrupole susceptibility extracted from our Raman spectra, and concomitant emergence of a collective mode associated with the spontaneous breaking of rotational symmetries. The quadrupolar order persists in the antiferromagnetic (AF) phase below $T_N \approx 230$ K, and becomes directly observable through its interference with the AF order in resonant x-ray diffraction, which allows us to uniquely determine its spatial structure. Further, we find using resonant inelastic x-ray scattering a complete breakdown of coherent magnon excitations at short-wavelength scales, suggesting a resonating-valence-bond-like quantum entanglement in the AF state^{11,12}. Taken together, our results reveal a quantum order underlying the Néel AF that is widely believed to be intimately connected to the mechanism of high temperature superconductivity (HTSC)¹³⁻¹⁵.

With its relevance to HTSC in cuprates, spin one-half ($S=1/2$) Heisenberg model on a square lattice has been a subject of extensive research over the last several decades^{10,14-16}. Although Mermin-Wagner theorem states that continuous symmetries cannot be spontaneously broken in two dimensions (2D), it is well established that Néel-type AF orders develop at low temperatures due to weak inter-layer couplings that form a 3D network in quasi-2D materials¹⁷. Nevertheless, spins retain much of their properties in the disordered phase and

undergo large quantum zero-point motions^{18,19}. The resulting ground state wave function is believed to embody a highly non-trivial structure akin to those in quantum spin liquids^{20,21}. For instance, the resonant valence bond (RVB), a superposition of states in which spins pair up to form singlet “valence bonds”, may have substantial overlap with the ground state¹³ (Fig. 1). Upon carrier doping, these singlets evolve into Cooper pairs in a prominent theory of HTSC^{13,14}.

What is not well known, however, is the fact that such quantum entanglement between a pair of nearest-neighbor (NN) spins can also manifest as an ordered spin quadrupole moment when spins are canted³⁻⁶ (Fig. 1). Because quadrupole moment can be non-zero only for $S \geq 1$, existence of a quadrupolar order in a $S=1/2$ system necessarily implies that spin pairs are entangled and have $S=1$ triplet components. Unlike singlets, however, a quadrupolar order is, in principle, measurable²²⁻²⁴ as it leads to spontaneous breaking of rotation symmetries^{25,26}. In this Article, we show that a quadrupolar order coexists with the Néel AF order in Sr₂IrO₄, a single-layer ($n=1$) member of the Ruddlesden-Popper series iridates (Fig. 2a), which has received much attention due to its similarities with superconducting cuprates in their phenomenology⁷⁻¹⁰. Furthermore, we show that it persists above T_N and realizes a SN phase.

I. CIRCULAR DICHROIC RESONANT X-RAY DIFFRACTION

We use resonant x-ray diffraction (RXD) to show the coexistence of a quadrupolar and a dipolar (canted AF) order (Fig. 2a). The dipole-quadrupole interference contribution to the RXD intensity can be isolated by measuring circular dichroic (CD) signal of a magnetic Bragg reflection defined as

$$I_{\text{CD}} = \frac{I_{\text{DIFF}}}{I_{\text{SUM}}} = \frac{I_{\text{LL}} + I_{\text{LR}} - I_{\text{RR}} - I_{\text{RL}}}{I_{\text{LL}} + I_{\text{LR}} + I_{\text{RR}} + I_{\text{RL}}}, \quad (1)$$

where $I_{\text{L(R)R(L)R}}$ denotes the intensity of left (right) cir-

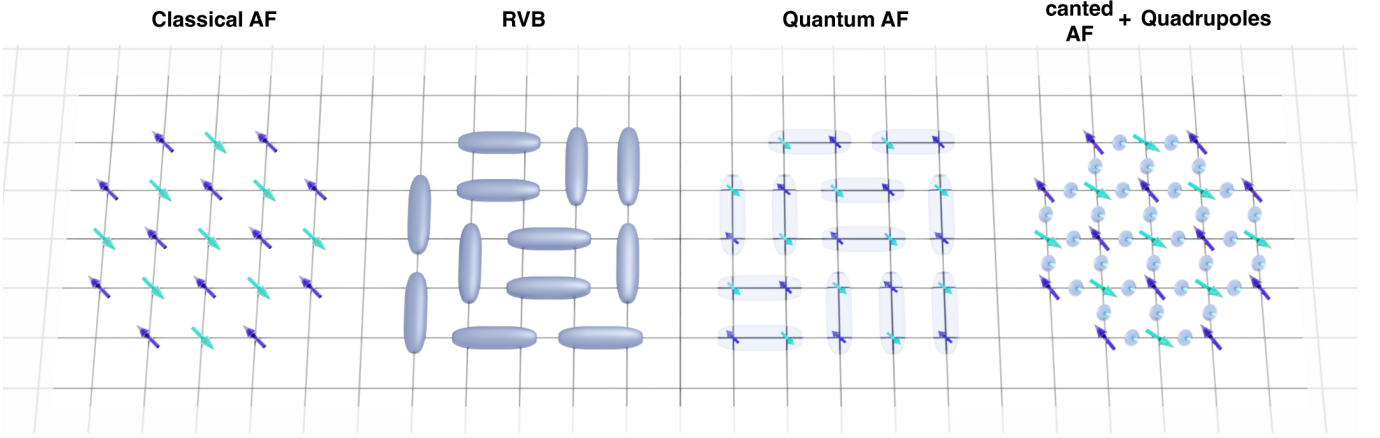


Fig. 1 | Spin one-half moments on a square lattice. In a strict 2D, AF order is not allowed at any finite temperature and spins are disordered but quantum entangled in a non-trivial way. For example, RVB is a state in which spins pair up to form singlets and fluctuate among numerous different configurations covering the square lattice with such dimers. Although most quasi-2D materials develop AF orders due to weak inter-layer couplings, spins still undergo strong quantum fluctuations. In a canted AF, quantum entanglement can manifest as an ordered spin quadrupole moment.

cular polarized incident x-ray scattered into left (right) circular outgoing x-ray. This definition of I_{CD} reflects the fact that the scattered x-ray polarization is not resolved in our experiment. It is straightforward to show that the difference spectrum (I_{DIFF}) in our particular case can be expressed as (see Supplementary Note S1)

$$I_{DIFF} \propto F_1^M e_1^A F_2^Q e_2^S + F_1^Q e_1^S F_2^M e_2^A - F_2^M e_1^A F_1^Q e_2^S - F_2^Q e_1^S F_1^M e_2^A, \quad (2)$$

where $F_{1,2}^Q$ and $F_{1,2}^M$ couple to symmetric (e_1^S) and antisymmetric (e_2^A) component of the polarization tensor $e_{\alpha\beta} \equiv \epsilon_{\alpha}^* \epsilon_{\beta}$, respectively, and represent the complex structure factor ($F \equiv F_1 + iF_2$) associated with time-reversal-even quadrupoles and time-reversal-odd dipoles, respectively. Thus, CD arises from the interference between dipolar and quadrupolar scatterings in the electric-dipole-electric-dipole ($E1-E1$) process of RXD. In Supplementary Note S2, we argue that this is the unique explanation for the CD in our case among all known mechanisms.

Figures 2b and 2c show the representative resonance profile of the (0021) reflection, arising from the net FM moment due to canting of the spins⁸, at two different azimuth angles (Ψ), defined as the angle between the crystallographic a -axis and the vertical scattering plane. I_{DIFF} is non-zero at and close to the resonance, and positive (negative) at $\Psi = 30^\circ$ ($\Psi = -56^\circ$). Figures 2d and 2e show I_{SUM} and I_{DIFF} at the resonance for the full range of Ψ measured. The Ψ -dependence of I_{CD} (Fig. 2f) allows us to determine the spatial structure and symmetry of the quadrupolar order. To systematically find all symmetry-allowed $\mathbf{q} = 0$ bond-centered quadrupole structures (see Supplementary Note S3), we first note that the reflection appearing at (0021) implies that both the dipolar

and the quadrupolar orders break the body-center translation symmetry. Such structures are represented by one of the four irreducible representations (IRs) Γ_1 , Γ_2 , Γ_3 , and Γ_4 , which are all 2D. For example, it is known that the magnetic structure shown in Fig. 2a belongs to Γ_1 IR²⁷.

While there are many different possible quadrupole structures (see Supplementary Note S3), there are only a few that have non-zero structure factors, which involve yz/zx quadrupoles for Γ_1 and Γ_2 , xy for Γ_3 , and $x^2 - y^2 / 3z^2 - r^2$ for Γ_4 . In Fig. 2f, the Ψ -dependence of I_{CD} is simulated for each of these structures and compared with the data. We find that only the Γ_1 structure, depicted in Fig. 2a, is consistent with the experimental data, whose key feature is the sign change at $\Psi = 0^\circ$. The total scattering amplitude is given by

$$F = F^M + rF^Q \quad (3)$$

$$= i \begin{pmatrix} 0 & 0 & -cM_y \\ 0 & 0 & c^*M_x \\ cM_y & -c^*M_x & 0 \end{pmatrix} + r \begin{pmatrix} 0 & 0 & cQ_{zx} \\ 0 & 0 & c^*Q_{yz} \\ cQ_{zx} & c^*Q_{yz} & 0 \end{pmatrix},$$

where $\mathbf{M} = (M_x, M_y)$ and $\mathbf{Q} = (Q_{yz}, Q_{zx})$ are 2D real basis vectors (whose transformation matrices are listed in Supplementary Note S3) for Γ_1 representing the net FM component of the magnetic order and the quadrupolar order, respectively, normalized to one when they have the maximal values; and $c = 4(1 - i)$ is a constant arising from the structure factor. r is a dimensionless factor accounting for the fact that quadrupoles only become visible by high-order RXD processes (see Supplementary Note S4 for possible microscopic mechanisms).

For the magnetic order, it is known that the easy axis is along $\langle 100 \rangle$ ²⁸, and the fact that I_{SUM} has a minimum at $\Psi = 0^\circ$ means that the magnetic domain being measured

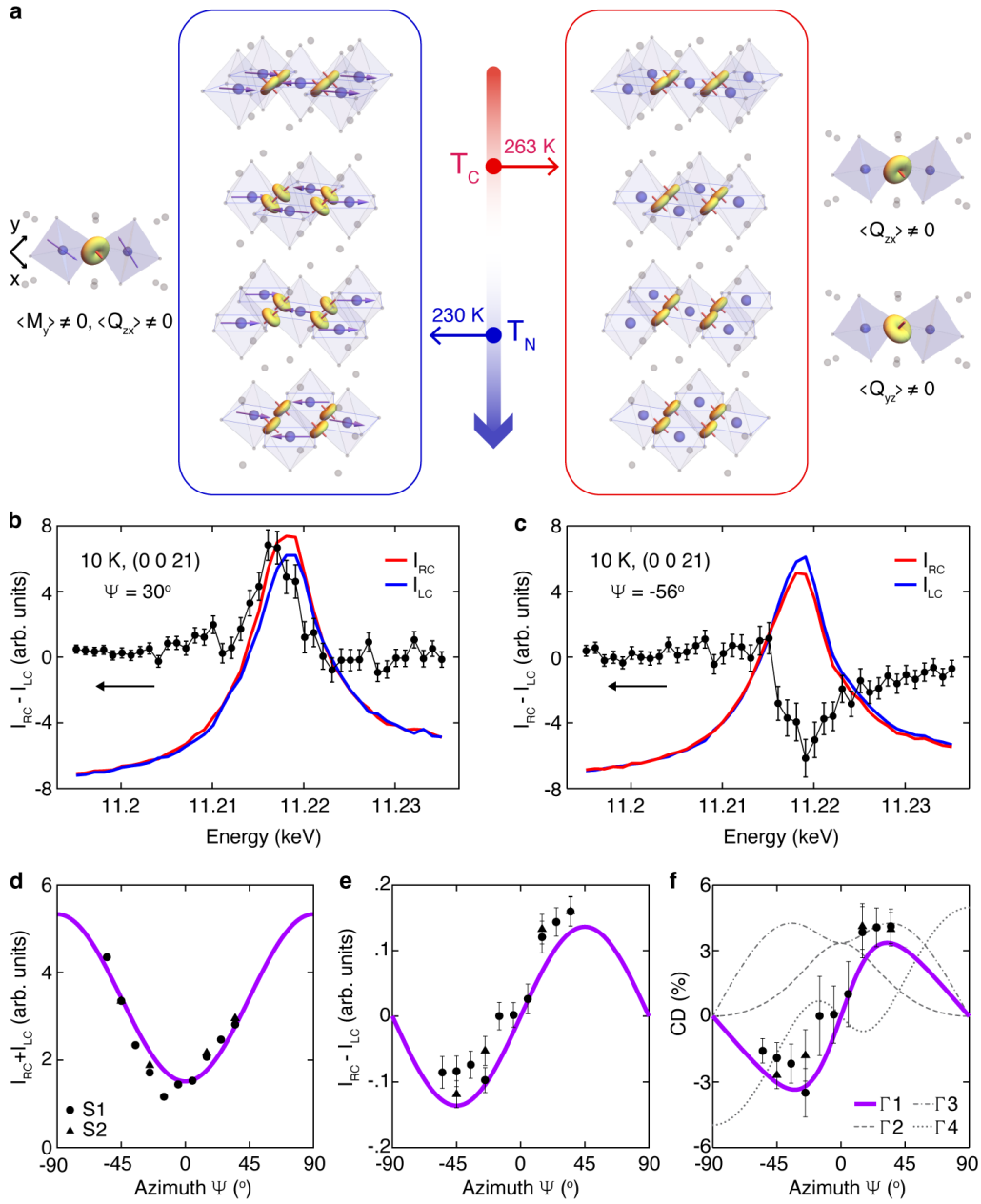


Fig. 2 | Dipole-quadrupole interference in CD-RXD. **a**, A schematic for the Néel and SN orders overlaid on the crystal structure of Sr_2IrO_4 having the tetragonal $I4_1/acd$ space group. The magnetic and quadrupole moments mutually constrain their orientations below T_N (left), whereas (Q_{zx}, Q_{yz}) transforms as an E_g doublet above T_N (right). **b, c**, Resonance profile of the circular dichroic signal at (0021) magnetic reflection, measured at $\Psi = 30^\circ$ (**b**) and $\Psi = -56^\circ$ (**c**). I_{RC} (red) and I_{LC} (blue) denote the diffraction intensity for right- and left-circularly polarized incident x-rays, respectively. **d, e**, $I_{\text{SUM}} \equiv I_{\text{RC}} + I_{\text{LC}}$ (**d**) and $I_{\text{DIFF}} \equiv I_{\text{RC}} - I_{\text{LC}}$ (**e**) at the resonance for the full range of Ψ measured. S1 and S2 are obtained from two independent measurements. **f**, Comparison of $I_{\text{CD}} \equiv I_{\text{DIFF}}/I_{\text{SUM}}$ to the simulations for different irreducible representations. The best fit to the data using Γ_1 profile is shown in **d-f**, and its structure is shown in **a**.

has the FM (AF) component along the b -(a -)axis, and hence $M_x = 0$. As we shall see below, fixing the direction of \mathbf{M} along y constrains Q_{yz} to be zero. Thus, it follows that

$$I_{\text{CD}} = \frac{(rQ_{zx}/M_y) \sin \alpha \sin 2\Psi}{1 - \cos 2\alpha \cos \Psi^2 + (rQ_{zx}/M_y)^2 \sin \Psi^2}, \quad (4)$$

where α is incidence angle to the sample surface ($\sim 27^\circ$). Thus, the data can be fit with rQ_{zx}/M_y as the only fitting parameter, and the best fit is obtained when $rQ_{zx}/M_y \approx 0.04$ (Fig. 2f). With a quantitative estimate of the r factor, which is beyond the scope of this work, one can in principle compare the relative magnitudes of

Q_{zx} and M_y .

II. TWO-SITE $S = 1/2$ MODEL

When a quadrupolar order coexists with a dipolar order, its allowed structure is constrained by the orientation of the dipolar order. For example, for a single $S = 1$ spin, it is easy to show that if its dipole moment is along z , then yz and zx quadrupole moments are zero. For the present case, we proceed with a simple two-site $S = 1/2$ model (see Supplementary Note S5). An arbitrary wavefunction for a pair of NN spins can be expressed in the singlet-triplet basis (s, T_x, T_y, T_z) in terms of two parameters θ and ϕ as $\mathbf{u} + i\mathbf{v}$, where

$$\begin{aligned} \mathbf{u} &= \cos\theta(\cos\phi\cos\phi_c, -\sin\phi, 0, \cos\phi\sin\phi_c), \\ \mathbf{v} &= \sin\theta(\sin\phi\cos\phi_c, \cos\phi, 0, \sin\phi\sin\phi_c), \end{aligned} \quad (5)$$

under the constraints that the AF(FM) component of the ordered moment is along $a(b)$ axis, and the canting angle $\phi_c \approx 12^\circ$; i.e., $\langle N_y \rangle = \langle N_z \rangle = \langle M_x \rangle = \langle M_z \rangle = 0$ and $\langle M_y \rangle / \langle N_x \rangle = \tan\phi_c$, (where $N_\alpha \equiv S_\alpha^1 - S_\alpha^2$ and $M_\alpha \equiv S_\alpha^1 + S_\alpha^2$).

Table 1 compares the magnitudes of magnetic and non-magnetic orders calculated as functions of θ and ϕ . First, we find that $\langle Q_{xy} \rangle = \langle Q_{yz} \rangle = 0$ for all values of θ and ϕ , but $\langle Q_{zx} \rangle$ can be nonzero only when ϕ_c is nonzero. This suggests that Dzyloshinskii-Moriya (DM) interaction plays an important role in stabilizing the quadrupolar order, since the spin canting arises from the same origin⁹. Second, it is clear that θ parameterizes the competition between the magnetic and nonmagnetic sectors. For example, at $\theta = \frac{\pi}{4}$ the magnetic moment fully saturates and $\langle Q_{zx} \rangle = 0$. Third, in the non-magnetic sector ϕ controls the magnitude of $\langle Q_{zx} \rangle$, which anti-correlates with that of the dimer correlation $\langle -\mathbf{S}^1 \cdot \mathbf{S}^2 - \frac{1}{4} \rangle$, which takes the values $\frac{1}{2}, 0, -\frac{1}{2}$ for the singlet, Néel AF state, and triplets, respectively. In other words, just as the net FM moment has its origin in the canting of AF spins, $\langle Q_{zx} \rangle$ arises from the underlying singlet correlation by ‘‘canting’’ in angle ϕ . This raises an intriguing possibility that a SN may arise from a smooth deformation of

Table 1 | Quadrupole and dipole moments from the two-site $S=1/2$ model calculation.

Type	Order	Expression
AF	$\langle N_x \rangle$	$\sin 2\theta \cos \phi_c$
FM	$\langle M_y \rangle$	$\sin 2\theta \sin \phi_c$
Quadrupole	$\langle Q_{zx} \rangle$	$\frac{1}{2} (\cos 2\theta \sin 2\phi \sin \phi_c)$
Singlet	$\langle -\mathbf{S}^1 \cdot \mathbf{S}^2 - \frac{1}{4} \rangle$	$\frac{1}{2} (\cos 2\theta \cos 2\phi \cos^2 \phi_c - \sin^2 \phi_c)$

a RVB state that has non-zero singlet correlation for every NN pair spins. For instance, recent studies find that rotating one of the spins by 180° in every dimer in a singlet RVB leads to a triplet RVB, which inherits some of the generic properties of the RVBs, such as quasiparticles with fractional quantum numbers^{29,30}.

III. RAMAN SPECTROSCOPY

Next, we use Raman spectroscopy, which has been suggested as a sensitive probe for SN³, to show that the quadrupolar order persists above T_N , armed with the information that the order should appear in the YZ or ZX polarization channel, which correspond to E_g symmetry channel of the tetragonal D_{4h} point group. This requires the laser beam to be incident on the side surface of a thin plate-like crystal, and thus has not been measured in previous Raman studies on Sr_2IrO_4 ^{31–33}. Figure 3a shows the Raman spectra measured in ZX scattering geometry. Upon cooling down from $T = 325$ K, we observe a broad quasi-elastic feature developing with its tail extending up to $\lesssim 10$ meV, which is indicative of slow fluctuations of spins (Fig. 3a). Integrating the Raman conductivity χ''/ω over a sufficiently large energy window (0.85 meV \sim 23.4 meV), we obtain in Fig. 3b the real part of the static susceptibility, which follows the Curie-Weiss temperature dependence with $T_C \approx 263$ K.

Concomitantly, an A_{1g} mode emerges (Fig. 3c and Extended Data Fig. 1), which is barely visible above our instrumental low-energy cutoff ≈ 0.85 meV at T_C , but upon further cooling becomes well resolved as the peak moves to higher energies. We interpret this peak as the phase mode associated with the quadrupolar order, analogous to spin-wave modes in the AF phase. The order parameter has E_g symmetry, which can be continuously rotated about the c -axis. This allows the phase mode to have the energy (1 \sim 2 meV) an order of magnitude smaller than the temperature scale of T_C (~ 20 meV), in accordance with the Goldstone theorem. Together with the divergence in the static susceptibility, this collective excitation constitutes direct evidence of a thermodynamic phase transition at $T_C \sim 263$ K, well above the AF transition temperature $T_N \sim 230$ K.

The A_{1g} mode persists as the sample is cooled down through T_N (Figs. 3c and 3d), at which temperature the B_{2g} single-magnon mode emerges (Fig. 3e). The A_{1g} mode becomes gapped close to T_N as the AF order further reinforces the breaking of the rotational symmetry (Fig. 3f). The intensity of the A_{1g} mode continues to grow in the AF phase (Fig. 3d), implying coexistence of dipolar and quadrupolar orders. As the AF order sets in, however, the stacking pattern of the quadrupoles changes, which is governed by weak inter-layer interactions of $\lesssim 10$ μeV energy scales, four orders of magnitudes smaller than those for intra-layer interactions²⁸ (Fig. 2a). We note that the A_{1g} mode is almost insensitive to the onset of the dipolar order, indicating that spins entan-

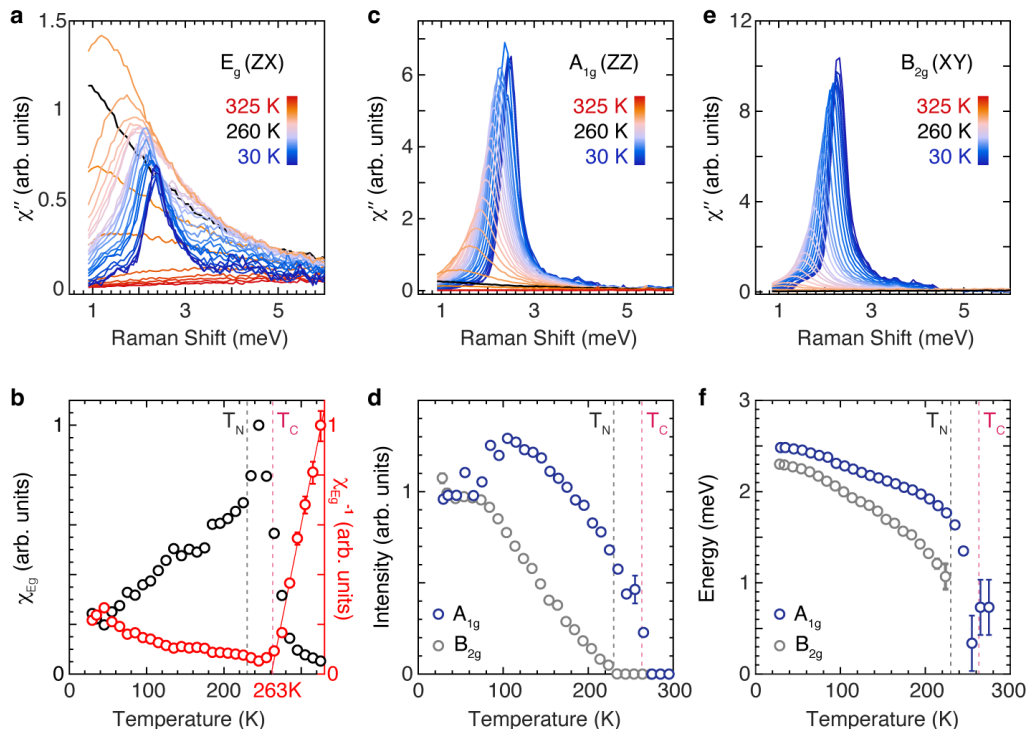


Fig. 3 | Phase transition into the spin-nematic phase. **a**, Raman spectra in the E_g symmetry channel measured on cooling. **b**, The real part of the uniform static susceptibility (black) obtained by integrating the E_g Raman conductivity χ''/ω . The inverse susceptibility (red) exhibits a Curie-Weiss behaviour with $T_C \simeq 263$ K. **c**, **e**, A_{1g} phase mode emerges at T_C (**c**), and the B_{2g} magnon below T_N (**e**). **d**, **f**, Temperature dependence of the intensities (**d**) and energies (**f**) of A_{1g} and B_{2g} modes extracted by fitting the spectra to Fano profiles $I(\omega) = \frac{I_0}{\Gamma(1-q^2)} \left(1 - \frac{(q+\epsilon)^2}{1+\epsilon^2}\right)$, where $\epsilon = (\omega - \omega_0)/\Gamma$, Γ is the linewidth, and q is the asymmetry parameter.

gument remains intact below T_N .

IV. POLARIZATION-RESOLVED RESONANT INELASTIC X-RAY SCATTERING

If the quadrupolar order comprises a substantial part of the ground state (small θ limit in Eq. 5), excitation spectra must exhibit a qualitative departure from the classical spin-wave theory (SWT), which largely reproduces the experimental spectra of cuprate square-lattice AFs^{19,34–36}. Figure 4 shows the RIXS spectra for the spin components transverse (T) and longitudinal (L) to the ordered moment direction, which we resolve by measuring the spectra for two different magnetic moment directions aligned using a small permanent magnet (see Extended Data Table 1 and Supplementary Note S6). At the ordering wavevector (π, π) (Fig. 4b), the spectral weight is mostly in the T channel, consistent with the SWT description, which expects a divergent intensity for a gapless Goldstone mode. The T magnon mode is also clearly visible at $(\pi/2, \pi/2)$, although a significant weight is transferred to the L channel (Fig. 4c). By contrast, at $(\pi, 0)$ the spectrum is completely isotropic and shows no sharp feature that can be identified as a magnon mode

(Fig. 4d).

In the cuprates, the ‘ $(\pi, 0)$ anomaly’ is ubiquitously observed across many different materials^{11,37–41}, and from its isotropic nature the continuum has been interpreted as deconfined fractional quasiparticles (spinons)^{11,12}. We note, however, that the T mode still constitutes the dominant part of the total intensity in most cases. To the best of our knowledge, the complete loss of the coherent magnon intensity is unprecedented, and renders alternative multi-magnon scenarios⁴² unlikely in our case. Rather, attributing the isotropic continuum to deconfined spinons in turn suggests that the quadrupolar order may be a byproduct of a RVB-like state.

V. DISCUSSION

Theoretically, SNs are predicted to arise in certain spin models with competing interactions^{1,43–46}. For example, in a square-lattice, four-spin exchange (J_c) competing with ferromagnetic (FM) NN Heisenberg exchange (J) can lead to a SN^{4,5}. In this regard, $5d$ transition-metal oxides, classified as ‘weak’ Mott insulators stabilized by strong spin-orbit coupling, may be a promising ground to search for a SN, because the large spatial extent of the

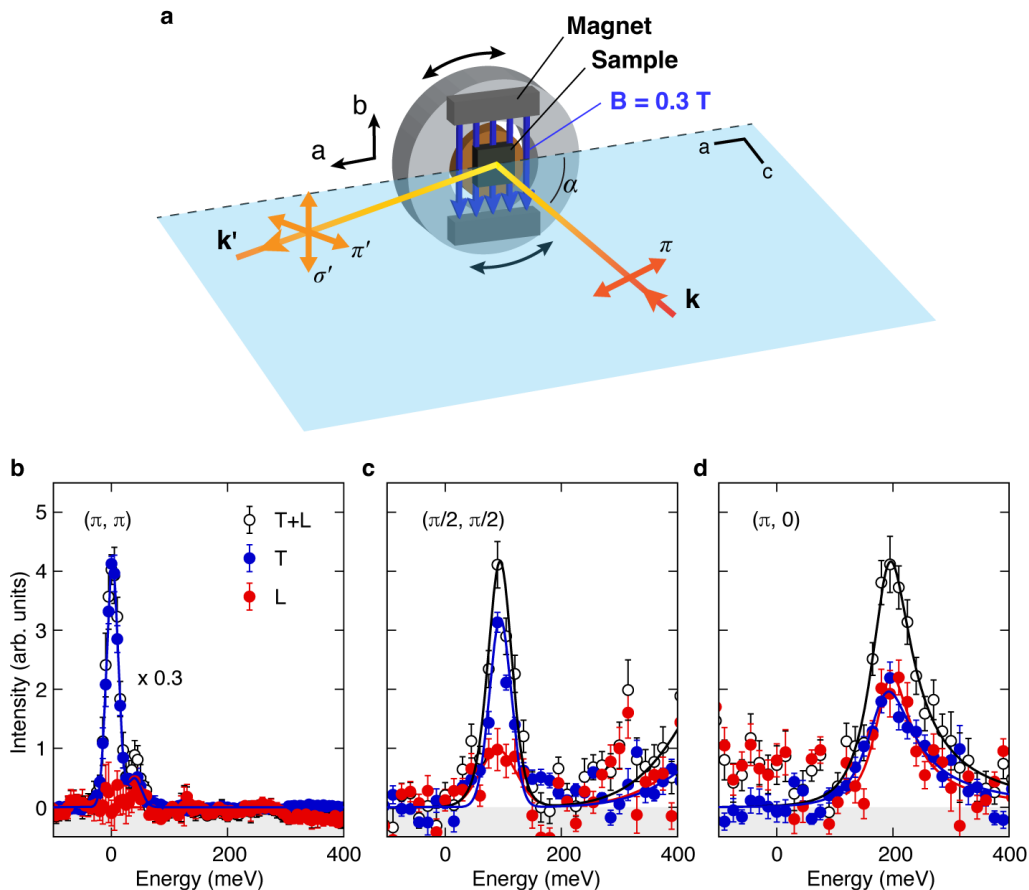


Fig. 4 | Complete breakdown of magnon at short wavelength scales. **a**, A schematic of the RIXS geometry. X-rays with π polarization are incident to the sample with the angle $\alpha \approx 75^\circ$, and scattered x-rays are collected without polarization analysis. A single crystal of Sr_2IrO_4 is placed between two permanent magnets that apply a magnetic field of 0.3 T along the b -axis (a -axis) at the sample position aligning the magnetic domains, i.e., $\mathbf{M} \parallel \hat{b}$ ($\mathbf{M} \parallel \hat{a}$). The direction of the applied field can be changed by rotating the outer disk on which the magnets are mounted while the sample stays fixed. The angle between the incident and outgoing x-rays is fixed close to 90° to suppress elastic Thomson scattering. **b-d**, RIXS spectra for (π, π) (**b**), $(\pi/2, \pi/2)$ (**c**), and $(\pi, 0)$ (**d**). The transverse mode (T) and the longitudinal mode (L) are displayed along with the sum of the two (T+L). Solid lines are guides to the eye. Each component is extracted from the raw spectra measured in different magnetic field directions with a fixed scattering geometry (see Extended Data Table 1 and Supplementary Note S6).

$5d$ orbitals can bring about strong competing interactions with NN Heisenberg interactions^{10,47}. Indeed, presence of interaction terms beyond NN in Sr_2IrO_4 is clear from its steep spin-wave dispersion along the magnetic zone-boundary⁴⁸, which can be equally well fitted with a model including J_c or further-neighbor couplings (J_2 and J_3). Further, our study suggests that the large canting angle of the spins resulting in a sizable net FM moment in each layer may be favourable for stabilizing the SN phase even in an Néel AF.

The fact that L edges of $5d$ transition-metal elements are in the hard x-ray regime with access to a wide region in the momentum space is also advantageous for direct detection of spin quadrupoles, as x-rays become sensitive to quadrupoles under resonance conditions^{23,24,49}. Most other experimental probes are insensitive to spin quadrupoles, and evidence for a SN has so far been indirectly provided from thermodynamic^{25,50} and nuclear

magnetic resonance measurements²⁶. In Sr_2IrO_4 , evidence for a symmetry breaking order above T_N has been found in studies using second harmonic generation⁵¹, inelastic neutron scattering⁵², and magnetic torque measurements⁵³. These studies suggest loop currents as the possible order. While our result is inconsistent with such a time-reversal symmetry breaking order (see Extended Data Fig. 2), it is possible that these experiments are probing yet another order of different nature.

Our results vividly demonstrate that multiple orders are intertwined even in the Mott insulating phase. The discovery of the SN phase is not only significant on its own, but also paves a new pathway to investigate the entanglement structure of quantum spins and the possible connection between SN and RVB through resonant x-ray scattering processes²⁴. The quantum entanglement between NN spins manifests as a spin quadrupolar order, and possibly accounts for the complete loss of coher-

ent magnons at momentum $(\pi, 0)$. This in turn suggests that the quadrupolar order may be exploited to follow the singlets formed by NN spins. Along this direction, if quadrupolar orders can be detected through charge-quadrupole interference, their temperature and doping

evolution can be followed in the absence of a magnetic order, with the ultimate goal of elucidating the relationship between the role of magnetic correlations in myriad exotic phases displayed by doped Mott insulators.

-
- * These authors contributed equally to this work.
 † bjkim6@postech.ac.kr
- ¹ M. Blume and Y. Y. Hsieh, “Biquadratic Exchange and Quadrupolar Ordering,” *J. Appl. Phys.* **40**, 1249–1249 (1969).
 - ² AF Andreev and IA Grishchuk, “Spin Nematics,” *Sov. Phys. JETP* **60**, 267 (1984).
 - ³ Frédéric Mila, “Closing in on a magnetic analog of liquid crystals,” *Physics* **10**, 64 (2017).
 - ⁴ A. Läuchli, J. C. Domenge, C. Lhuillier, P. Sindzingre, and M. Troyer, “Two-Step Restoration of SU(2) Symmetry in a Frustrated Ring-Exchange Magnet,” *Phys. Rev. Lett.* **95**, 137206 (2005).
 - ⁵ Nic Shannon, Tsutomu Momoi, and Philippe Sindzingre, “Nematic Order in Square Lattice Frustrated Ferromagnets,” *Phys. Rev. Lett.* **96**, 027213 (2006).
 - ⁶ Masahiro Sato, Toshiya Hikihara, and Tsutomu Momoi, “Spin-Nematic and Spin-Density-Wave Orders in Spatially Anisotropic Frustrated Magnets in a Magnetic Field,” *Phys. Rev. Lett.* **110**, 077206 (2013).
 - ⁷ B. J. Kim, Hosub Jin, S. J. Moon, J.-Y. Kim, B.-G. Park, C. S. Leem, Jaejun Yu, T. W. Noh, C. Kim, S.-J. Oh, J.-H. Park, V. Durairaj, G. Cao, and E. Rotenberg, “Novel $J_{\text{eff}} = 1/2$ Mott State Induced by Relativistic Spin-Orbit Coupling in Sr_2IrO_4 ,” *Phys. Rev. Lett.* **101**, 076402 (2008).
 - ⁸ B. J. Kim, H. Ohsumi, T. Komesu, S. Sakai, T. Morita, H. Takagi, and T. Arima, “Phase-Sensitive Observation of a Spin-Orbital Mott State in Sr_2IrO_4 ,” *Science* **323**, 1329–1332 (2009).
 - ⁹ G. Jackeli and G. Khaliullin, “Mott Insulators in the Strong Spin-Orbit Coupling Limit: From Heisenberg to a Quantum Compass and Kitaev Models,” *Phys. Rev. Lett.* **102**, 017205 (2009).
 - ¹⁰ Joel Bertinshaw, Y. K. Kim, Giniyat Khaliullin, and B. J. Kim, “Square Lattice Iridates,” *Annu. Rev. Condens. Matter Phys.* **10**, 315–336 (2019).
 - ¹¹ B. Dalla Piazza, M. Mourigal, N. B. Christensen, G. J. Nilsen, P. Tregenna-Piggott, T. G. Perring, M. Enderle, D. F. McMorrow, D. A. Ivanov, and H. M. Rønnow, “Fractional Excitations in the Square-Lattice Quantum Antiferromagnet,” *Nat. Phys.* **11**, 62–68 (2015).
 - ¹² Hui Shao, Yan Qi Qin, Sylvain Capponi, Stefano Chesi, Zi Yang Meng, and Anders W. Sandvik, “Nearly Deconfined Spinon Excitations in the Square-Lattice Spin-1/2 Heisenberg Antiferromagnet,” *Phys. Rev. X* **7**, 041072 (2017).
 - ¹³ P. W. Anderson, “The Resonating Valence Bond State in La_2CuO_4 and Superconductivity,” *Science* **235**, 1196–1198 (1987).
 - ¹⁴ Patrick A. Lee, Naoto Nagaosa, and Xiao-Gang Wen, “Doping a Mott Insulator: Physics of High-temperature Superconductivity,” *Rev. Mod. Phys.* **78**, 17–85 (2006).
 - ¹⁵ B. Keimer, S. A. Kivelson, M. R. Norman, S. Uchida, and J. Zaanen, “From quantum matter to high-temperature superconductivity in copper oxides,” *Nature* **518**, 179–186 (2015).
 - ¹⁶ D. J. Scalapino, “A common thread: The pairing interaction for unconventional superconductors,” *Rev. Mod. Phys.* **84**, 1383–1417 (2012).
 - ¹⁷ D. Vaknin, S. K. Sinha, D. E. Moncton, D. C. Johnston, J. M. Newsam, C. R. Safinya, and H. E. King, “Antiferromagnetism in $\text{La}_2\text{CuO}_{4-y}$,” *Phys. Rev. Lett.* **58**, 2802–2805 (1987).
 - ¹⁸ Rajiv R. P. Singh, “Thermodynamic parameters of the $T=0$, spin-1/2 square-lattice Heisenberg antiferromagnet,” *Phys. Rev. B* **39**, 9760–9763 (1989).
 - ¹⁹ R. Coldea, S. M. Hayden, G. Aeppli, T. G. Perring, C. D. Frost, T. E. Mason, S.-W. Cheong, and Z. Fisk, “Spin Waves and Electronic Interactions in La_2CuO_4 ,” *Phys. Rev. Lett.* **86**, 5377–5380 (2001).
 - ²⁰ Lucile Savary and Leon Balents, “Quantum Spin Liquids: a Review,” *Rep. Prog. Phys.* **80**, 016502 (2016).
 - ²¹ Yi Zhou, Kazushi Kanoda, and Tai-Kai Ng, “Quantum Spin Liquid States,” *Rev. Mod. Phys.* **89**, 025003 (2017).
 - ²² V. Barzykin and L. P. Gor’kov, “Possibility of Observation of Nontrivial Magnetic Order by Elastic Neutron Scattering in Magnetic Field,” *Phys. Rev. Lett.* **70**, 2479–2482 (1993).
 - ²³ Andrew Smerald and Nic Shannon, “Theory of Spin Excitations in a Quantum Spin-nematic State,” *Phys. Rev. B* **88**, 184430 (2013).
 - ²⁴ Lucile Savary and T. Senthil, “Probing Hidden Orders with Resonant Inelastic X-Ray Scattering,” *arXiv:1506.04752* (2015).
 - ²⁵ Yoshimitsu Kohama, Hajime Ishikawa, Akira Matsuo, Koichi Kindo, Nic Shannon, and Zenji Hiroi, “Possible Observation of Quantum Spin-nematic Phase in a Frustrated Magnet,” *Proc. Natl. Acad. Sci. U.S.A.* **116**, 10686–10690 (2019).
 - ²⁶ A. Orlova, E. L. Green, J. M. Law, D. I. Gorbunov, G. Chanda, S. Krämer, M. Horvatic, R. K. Kremer, J. Wosnitza, and G. L. J. A. Rikken, “Nuclear Magnetic Resonance Signature of the Spin-Nematic Phase in LiCuVO_4 at High Magnetic Fields,” *Phys. Rev. Lett.* **118**, 247201 (2017).
 - ²⁷ Feng Ye, Songxue Chi, Bryan C. Chakoumakos, Jaime A. Fernandez-Baca, Tongfei Qi, and G. Cao, “Magnetic and Crystal Structures of Sr_2IrO_4 : A Neutron Diffraction Study,” *Phys. Rev. B* **87**, 140406 (2013).
 - ²⁸ J. Porras, J. Bertinshaw, H. Liu, G. Khaliullin, N. H. Sung, J. W. Kim, S. Francoual, P. Steffens, G. Deng, M. Moretti Sala, A. Efimenko, A. Said, D. Casa, X. Huang, T. Gog, J. Kim, B. Keimer, and B. J. Kim, “Pseudospin-Lattice Coupling in the Spin-Orbit Mott Insulator Sr_2IrO_4 ,” *Phys. Rev. B* **99**, 085125 (2019).
 - ²⁹ Elio J. König, Yashar Komijani, and Piers Coleman, “Triplet Resonating Valence Bond Theory and Transition Metal Chalcogenides,” *Phys. Rev. B* **105**, 075142 (2022).

- ³⁰ Ryuichi Shindou and Tsutomu Momoi, “ $SU(2)$ Slave-boson Formulation of Spin Nematic States in $S = \frac{1}{2}$ Frustrated Ferromagnets,” *Phys. Rev. B* **80**, 064410 (2009).
- ³¹ Mehmet Fatih Cetin, Peter Lemmens, Vladimir Gnezdilov, Dirk Wulferding, Dirk Menzel, Tomohiro Takayama, Kei Ohashi, and Hidenori Takagi, “Crossover from Coherent to Incoherent Scattering in Spin-Orbit Dominated Sr_2IrO_4 ,” *Phys. Rev. B* **85**, 195148 (2012).
- ³² Y. Gim, A. Sethi, Q. Zhao, J. F. Mitchell, G. Cao, and S. L. Cooper, “Isotropic and Anisotropic Regimes of the Field-dependent Spin Dynamics in Sr_2IrO_4 : Raman Scattering Studies,” *Phys. Rev. B* **93**, 024405 (2016).
- ³³ H. Gretarsson, N. H. Sung, M. Höppner, B. J. Kim, B. Keimer, and M. Le Tacon, “Two-Magnon Raman Scattering and Pseudospin-Lattice Interactions in Sr_2IrO_4 and $Sr_3Ir_2O_7$,” *Phys. Rev. Lett.* **116**, 136401 (2016).
- ³⁴ G. Aeppli, S. M. Hayden, H. A. Mook, Z. Fisk, S.-W. Cheong, D. Rytz, J. P. Remeika, G. P. Espinosa, and A. S. Cooper, “Magnetic dynamics of La_2CuO_4 and $La_{2-x}Ba_xCuO_4$,” *Phys. Rev. Lett.* **62**, 2052–2055 (1989).
- ³⁵ L. Braicovich, M. Minola, G. Dellea, M. Le Tacon, M. Moretti Sala, C. Morawe, J.-Ch. Peffen, R. Suprunangnet, F. Yakhou, G. Ghiringhelli, and N. B. Brookes, “The Simultaneous Measurement of Energy and Linear Polarization of the Scattered Radiation in Resonant Inelastic Soft X-ray Scattering,” *Rev. Sci. Instrum.* **85**, 115104 (2014).
- ³⁶ Y. Y. Peng, G. Dellea, M. Minola, M. Conni, A. Amorese, D. Di Castro, G. M. De Luca, K. Kummer, M. Salluzzo, X. Sun, X. J. Zhou, G. Balestrino, M. Le Tacon, B. Keimer, L. Braicovich, N. B. Brookes, and G. Ghiringhelli, “Influence of Apical Oxygen on the Extent of In-Plane Exchange Interaction in Cuprate Superconductors,” *Nat. Phys.* **13**, 1201–1206 (2017).
- ³⁷ N. B. Christensen, H. M. Rønnow, D. F. McMorrow, A. Harrison, T. G. Perring, M. Enderle, R. Coldea, L. P. Regnault, and G. Aeppli, “Quantum Dynamics and Entanglement of Spins on a Square Lattice,” *Proc. Natl. Acad. Sci. U.S.A.* **104**, 15264–15269 (2007).
- ³⁸ N. S. Headings, S. M. Hayden, R. Coldea, and T. G. Perring, “Anomalous High-Energy Spin Excitations in the High- T_c Superconductor-Parent Antiferromagnet La_2CuO_4 ,” *Phys. Rev. Lett.* **105**, 247001 (2010).
- ³⁹ Leonardo Martinelli, Davide Betto, Kurt Kummer, Riccardo Arpaia, Lucio Braicovich, Daniele Di Castro, Nicholas B. Brookes, Marco Moretti Sala, and Giacomo Ghiringhelli, “Fractional Spin Excitations in the Infinite-Layer Cuprate $CaCuO_2$,” *Phys. Rev. X* **12**, 021041 (2022).
- ⁴⁰ N. Tsyrlin, T. Pardini, R. R. P. Singh, F. Xiao, P. Link, A. Schneidewind, A. Hiess, C. P. Landee, M. M. Turnbull, and M. Kenzelmann, “Quantum Effects in a Weakly Frustrated $S = 1/2$ Two-Dimensional Heisenberg Antiferromagnet in an Applied Magnetic Field,” *Phys. Rev. Lett.* **102**, 197201 (2009).
- ⁴¹ N. Tsyrlin, F. Xiao, A. Schneidewind, P. Link, H. M. Rønnow, J. Gavilano, C. P. Landee, M. M. Turnbull, and M. Kenzelmann, “Two-Dimensional Square-Lattice $S = \frac{1}{2}$ Antiferromagnet $Cu(pz)_2(ClO_4)_2$,” *Phys. Rev. B* **81**, 134409 (2010).
- ⁴² Michael Powalski, Kai P. Schmidt, and Götz S. Uhrig, “Mutually attracting spin waves in the square-lattice quantum antiferromagnet,” *SciPost Phys.* **4**, 001 (2018).
- ⁴³ H. H. Chen and Peter M. Levy, “Quadrupole Phase Transitions in Magnetic Solids,” *Phys. Rev. Lett.* **27**, 1383–1385 (1971).
- ⁴⁴ P. Chandra and P. Coleman, “Quantum spin nematics: Moment-free magnetism,” *Phys. Rev. Lett.* **66**, 100–103 (1991).
- ⁴⁵ Andreas Läuchli, Frédéric Mila, and Karlo Penc, “Quadrupolar Phases of the $S = 1$ Bilinear-Biquadratic Heisenberg Model on the Triangular Lattice,” *Phys. Rev. Lett.* **97**, 087205 (2006).
- ⁴⁶ M. E. Zhitomirsky and H. Tsunetsugu, “Magnon pairing in quantum spin nematic,” *EPL* **92**, 37001 (2010).
- ⁴⁷ William Witczak-Krempa, Gang Chen, Yong Baek Kim, and Leon Balents, “Correlated Quantum Phenomena in the Strong Spin-Orbit Regime,” *Annu. Rev. Condens. Matter Phys.* **5**, 57–82 (2014).
- ⁴⁸ Jung-ho Kim, D. Casa, M. H. Upton, T. Gog, Young-June Kim, J. F. Mitchell, M. Van Veenendaal, M. Daghofer, J. Van Den Brink, G. Khaliullin, and B. J. Kim, “Magnetic Excitation Spectra of Sr_2IrO_4 Probed by Resonant Inelastic X-Ray Scattering: Establishing Links to Cuprate Superconductors,” *Phys. Rev. Lett.* **108**, 177003 (2012).
- ⁴⁹ D. F. McMorrow, K. A. McEwen, U. Steigenberger, H. M. Rønnow, and F. Yakhou, “X-Ray Resonant Scattering Study of the Quadrupolar Order in UPd_3 ,” *Phys. Rev. Lett.* **87**, 057201 (2001).
- ⁵⁰ M. Mourigal, M. Enderle, B. Fåk, R. K. Kremer, J. M. Law, A. Schneidewind, A. Hiess, and A. Prokofiev, “Evidence of a Bond-Nematic Phase in $LiCuVO_4$,” *Phys. Rev. Lett.* **109**, 027203 (2012).
- ⁵¹ K. L. Seyler, A. de la Torre, Z. Porter, E. Zoghlin, R. Polski, M. Nguyen, S. Nadj-Perge, S. D. Wilson, and D. Hsieh, “Spin-orbit-enhanced magnetic surface second-harmonic generation in Sr_2IrO_4 ,” *Phys. Rev. B* **102**, 201113 (2020).
- ⁵² Jaehong Jeong, Yvan Sidis, Alex Louat, Véronique Brouet, and Philippe Bourges, “Time-reversal Symmetry Breaking Hidden Order in $Sr_2(Ir,Rh)O_4$,” *Nat. Commun.* **8**, 15119 (2017).
- ⁵³ H. Murayama, K. Ishida, R. Kurihara, T. Ono, Y. Sato, Y. Kasahara, H. Watanabe, Y. Yanase, G. Cao, Y. Mizukami, T. Shibauchi, Y. Matsuda, and S. Kasahara, “Bond Directional Anapole Order in a Spin-Orbit Coupled Mott Insulator $Sr_2(Ir_{1-x}Rh_x)O_4$,” *Phys. Rev. X* **11**, 011021 (2021).
- ⁵⁴ Jimin Kim, Hoon Kim, Hyun-Woo J. Kim, Sunwook Park, Jin-Kwang Kim, Junyoung Kwon, Jung-ho Kim, Hyeong Woo Seo, Jun Sung Kim, and B. J. Kim, “Single crystal growth of iridates without platinum impurities,” *Phys. Rev. Mater.* **6**, 103401 (2022).
- ⁵⁵ D. Torchinsky, H. Chu, L. Zhao, N. B. Perkins, Y. Sizyuk, T. Qi, G. Cao, and D. Hsieh, “Structural Distortion-Induced Magnetoelastic Locking in Sr_2IrO_4 Revealed through Nonlinear Optical Harmonic Generation,” *Phys. Rev. Lett.* **114**, 096404 (2015).
- ⁵⁶ X. D. Zhu, R. Ullah, and V. Taufour, “Oblique-incidence Sagnac interferometric scanning microscope for studying magneto-optic effects of materials at low temperatures,” *Rev. Sci. Instrum.* **92**, 043706 (2021).

METHODS

Crystal Growth Single crystals of Sr_2IrO_4 were grown by the standard flux growth method. Powders of

IrO₂, SrCO₃, and SrCl₂ · 6H₂O were mixed and placed in an iridium crucible covered with a lid. The mixture was melted and soaked at $T = 1300^\circ\text{C}$, slowly cooled down to 900°C at $8^\circ\text{C}/\text{h}$, and then furnace cooled to room temperature. We note that our crystals grown in an iridium crucible have the lattice structure of space group $I4_1/acd$ (ref. 54) and shows no sign of glide symmetry breaking distortions previously reported⁵⁵.

Resonant x-ray diffraction (RXD) RXD experiments were carried out at the 1C beamline of Pohang Accelerator Laboratory and 4-ID-D beamline of the Advanced Photon Source. Incident x-ray was tuned at the Ir L_3 edge (11.217 keV). The focused beam having spatial resolution better than $\sim 100 \mu\text{m}$ was used. The sample was mounted on the cold finger of a closed-cycle cryostat and temperature was kept at 10 K throughout the experiment. The left and right circular polarized x-ray was generated using a diamond phase retarder. The helicity was switched at every data point to measure the flipping ratio of circular dichroic signal.

Resonant inelastic x-ray scattering RIXS spectra were measured at the 27-ID-B beamline of the Advanced Photon Source. Incident x-ray was tuned to the Ir L_3 edge (11.215 keV). Using a diamond (111) high-heat-load monochromator in combination with a Si (844) channel-cut monochromator reduced the energy band-pass down to 14.8 meV. The beam was then focused by a set of Kirkpatrick-Baez mirrors, producing a spot size of $40 \times 10 (\text{H} \times \text{V}) \mu\text{m}^2$ FWHM at the sample position. Scattered photons were analyzed by a Si (844) diced spherical analyzer with a radius of 2 m and with a mask of 2 cm diameter. The overall energy resolution was about 30 meV. A horizontal scattering geometry was used with the incident π -polarization and the outgoing polarization was not resolved. All RIXS spectra were taken around (3 0 28.5) in a normal incident scattering geometry and a small magnetic field ($\sim 0.3 \text{ T}$) was applied along the either a - or b -axis to align magnetic moments. The scattering angle (2θ) was kept around 90° to suppress elastic Thomson scatterings.

Raman spectroscopy Raman spectroscopy was performed with a home-built setup equipped with a 633 nm He-Ne laser and a liquid nitrogen cooled CCD (Princeton instruments). The elastic signal is removed by grating-based notch filters (Optigrate, BragGrateTM Notch filters). The spectra were acquired on as-grown surfaces of Sr₂IrO₄ crystals mounted in a closed cycle optical cryostat (Montana instruments). The laser power and beam spot size are 0.8 mW and $2 \mu\text{m}$, respectively, which resulted in an almost temperature independent laser heating of 25 K as determined from the Stokes to Anti-Stokes intensity ratio. All Raman spectra are Bose-corrected.

Magneto-optical Kerr measurement We performed magneto-optical Kerr measurements on Sr₂IrO₄ using an oblique-incidence zero-area Sagnac interferometer operating at 1550 nm wavelength to measure the in-plane

magnetization⁵⁶. The relative Kerr angle $\Delta\theta_K$ is obtained by subtracting temperature-independent backgrounds, coming from the instrumentation offset, measured at $T = 300 \text{ K}$, and converted to magnetization (in μ_B/ion) by a quantitative comparison of our 0.35 T Kerr data with the corresponding magnetization data in the Ref. 28. Throughout the measurements, the incident optical power was maintained below 1 mW so that the effect of optical heating was smaller than 1 K.

ACKNOWLEDGMENTS

We thank Nic Shannon, Giniyat Khaliullin and Yong Baek Kim for helpful discussions. This project is supported by IBS-R014-A2 and National Research Foundation (NRF) of Korea through the SRC (No. 2018R1A5A6075964). The use of the Advanced Photon Source at the Argonne National Laboratory was supported by the U. S. DOE under Contract No. DE-AC02-06CH11357. G.Y.C. is supported by the NRF of Korea (Grant No. 2020R1C1C1006048) funded by the Korean Government (MSIT) as well as the Institute of Basic Science under project code IBS-R014-D1. G.Y.C. is also supported by the Air Force Office of Scientific Research under Award No. FA2386-22-1-4061 and G.Y.C. also acknowledges Samsung Science and Technology Foundation under Project Number SSTF-BA2002-05. H.H. and J.J. are supported by the National Research Foundation of Korea (Grant No. 2020R1A5A1016518), and the Creative-Pioneering Researchers Program through Seoul National University.

AUTHORS CONTRIBUTIONS

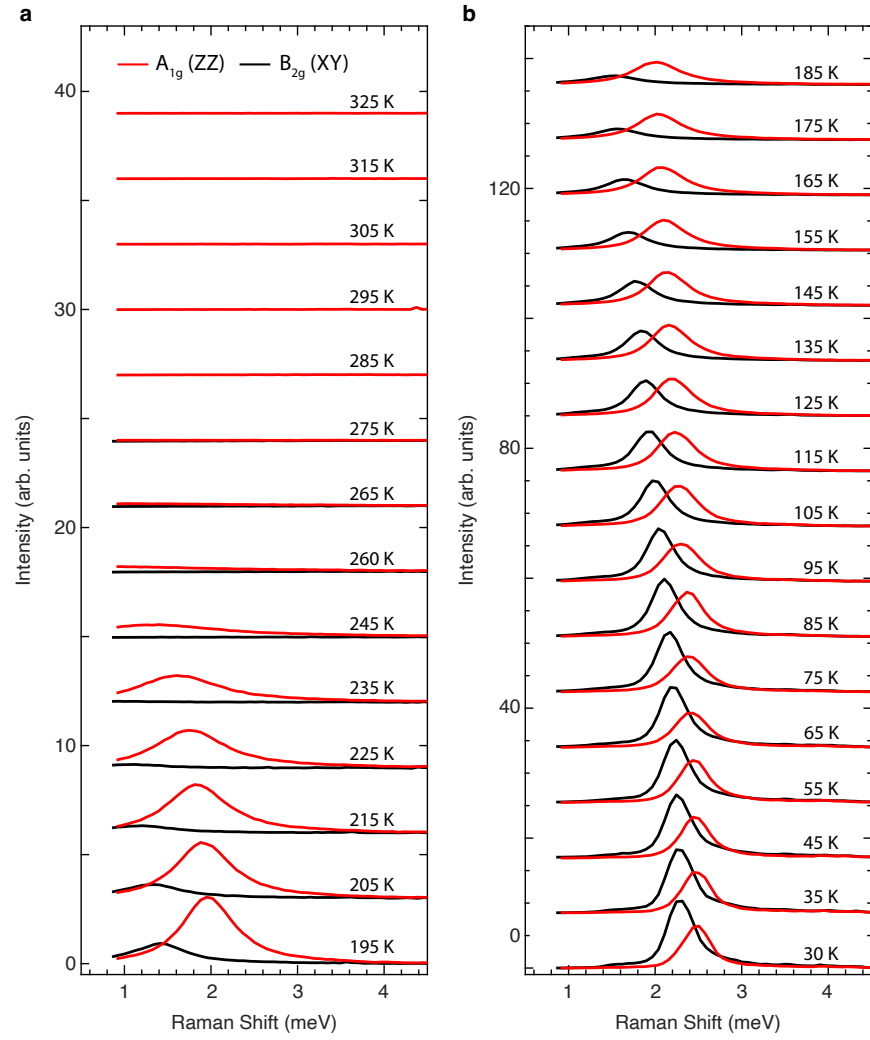
B.J.K. conceived and managed the project. H.K., K.K. and Jo.K. performed Raman experiments. H.K., S.H., J.S., G.F., Y.C., D.H. and J.W.K. performed RXD experiments. H.K., J.-K.K., H.-W.J.K. and Ju.K. performed RIXS experiments and analyzed the data. Ji.K. grew single crystals. H.H. and J.J. performed Kerr measurements. H.K. and B.J.K. performed representation analysis. W.L. and G.Y.C. assisted interpretation of the data. H.K., J.-K.K. and B.J.K. wrote the manuscript with inputs from all authors.

COMPETING INTERESTS

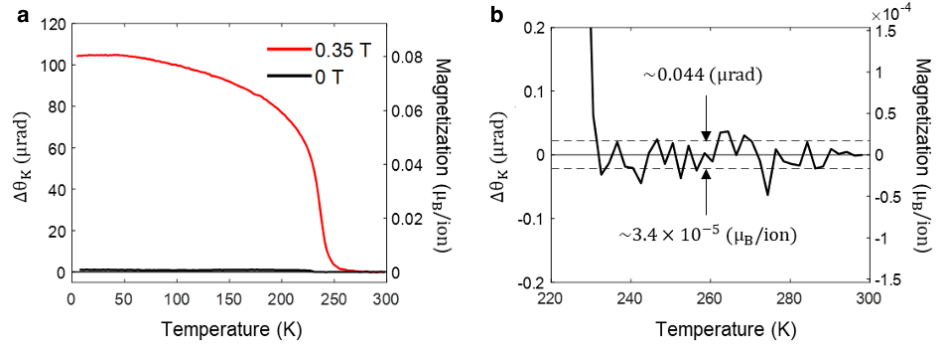
The authors declare no competing interests.

DATA AND MATERIALS AVAILABILITY

All data is available in the manuscript or the supplementary information.



Extended Data Fig. 1 | Temperature evolution of the low-energy Raman modes. The Raman spectra of the A_{1g} and B_{2g} modes shown in Figs. 2c and 2e are displayed with vertical offset for clarity. The A_{1g} (red) and B_{2g} (black) spectra were measured on the same crystal under the same experimental conditions including laser power and acquisition time, and the spectra are plotted in the same arbitrary unit.



Extended Data Fig. 2 | Magneto-optical Kerr measurement. **a**, Relative Kerr angle in the 0.35 T in-plane magnetic field (red line) and ambient magnetic field near 0 T (black line). The relative Kerr angle (left axis) is converted to magnetization (right axis) using a conversion factor of 7.7×10^{-4} ($\mu_B/\text{Ir ion}$)/(μrad). **b**, Magnified plot of the 0 T data in **a**. Dashed line indicates the standard deviation for the $T = 230 \sim 300$ K range. The Kerr signal at $B = 0$ T in the range of $230 \text{ K} < T < 300$ K shows that no net magnetization is present within our experimental resolution, 3.4×10^{-5} μ_B/ion (dashed line), thus confirming the preservation of time-reversal symmetry above $T_N \sim 230$ K.

Extended Data Table 1 | Sensitive mode for each combination of specific scattering geometry and field direction in RIXS measurements on Sr_2IrO_4 . Here, L stands for the longitudinal mode, T for the in-plane transverse mode, and T' for the out-of-plane transverse mode. Please note that 'Mode' represents the most sensitive mode in a specific scattering geometry and a field direction.

Incident angle	Field direction	Moment direction	Polarization	Sensitive element	Mode
Normal	[100]	[010]	$e_\pi \times e_{\pi'}$	[010]	L
			$e_\pi \times e_{\sigma'}$	[001]	T'
	[010]	[100]	$e_\pi \times e_{\pi'}$	[010]	T
			$e_\pi \times e_{\sigma'}$	[001]	T'
Grazing	[100]	[010]	$e_\pi \times e_{\pi'}$	[010]	L
			$e_\pi \times e_{\sigma'}$	[100]	T
	[010]	[100]	$e_\pi \times e_{\pi'}$	[010]	T
			$e_\pi \times e_{\sigma'}$	[100]	L